IEEE Access
Multidisciplinary | Rapid Review | Open Access Journal

Received March 18, 2022, accepted April 23, 2022, date of publication May 18, 2022, date of current version June 10, 2022.

Digital Object Identifier 10.1109/ACCESS.2022.3176366

Reduced Sensor-Based Harmonic Resonance Detection and its Compensation in Power Distribution System With SAPF

SHIVANGNI SHARMA[1], VIMLESH VERMA[1], (Senior Member, IEEE), MOHD TARIQ[2], (Senior Member, IEEE), AND SHABANA UROOJ[3], (Senior Member, IEEE)

[1]Department of Electrical Engineering, National Institute of Technology Patna, Patna 800005, India
[2]Department of Electrical Engineering, ZHCET, Aligarh Muslim University, Aligarh 202002, India
[3]Department of Electrical Engineering, College of Engineering, Princess Nourah bint Abdulrahman University, P.O. Box 84428, Riyadh-11671, Saudi Arabia

Corresponding authors: Mohd Tariq (tariq.ee@zhcet.ac.in) and Shabana Urooj (smurooj@pnu.edu.sa)

Princess Nourah bint Abdulrahman University Researchers Supporting Project, Princess Nourah bint Abdulrahman University, Riyadh, Saudi Arabia, under Grant PNURSP2022R79.

ABSTRACT Shunt Active Power Filter (SAPF) is widely used for harmonics and reactive power compensation. However, in addition to the harmonics, harmonic resonance also exists in the network, which is prominent in configurations where both SAPF and capacitor bank are present in the distribution network. Resonance is mainly caused due to interaction between line impedances, capacitor banks and modern electronic equipment with capacitive behaviour. Harmonic resonance leads to an increase in harmonic level around the resonance frequency, which further increases the overall THD of the distribution system. As there can be multiple resonance scenarios which may also vary depending on internal switching of capacitor devices, it is difficult for conventional SAPF to address both harmonic resonance and current harmonics. Therefore, to improve the overall power quality, it is important to first identify/detect and then selectively damp the detected harmonic resonance in the distribution network. Detection of resonance with SAPF commonly require external signal injection, additional circuitry and sensors. This paper deals with non-invasive machine learning (ML)-based resonance detection, which only requires voltage harmonics at the point of common coupling (PCC) as input. Hence, it eliminates the need for any modification in existing control strategy, external signal injection and additional sensors. Also, Resonance detection, resonance damping and harmonic compensation is achieved by utilising only two types of sensors i.e., voltage at PCC and load current.

INDEX TERMS Active power filters, harmonics, classification learning, power quality.

I. INTRODUCTION

Harmonic resonance is a power quality issue in power distribution networks that arises primarily due to interaction of line impedances, capacitor banks and modern power electronic loads [1], [2]. The main reason behind the increasing resonance issue is the capacitive behaviour of new energy-efficient household electronic equipment and the capacitor banks [3]. However, presence of resonance is more predominant in the case where Shunt Active Power Filter (SAPF) is installed in the system with the capacitor bank. SAPF is one of the most sought-after solution for power quality issues along with other configurations of Active Power Filter (APF)[4]. Capacitor banks are used as a Power Factor Correction (PFC) unit whereas SAPF is widely utilized to address both harmonic as well as reactive power issues. Harmonic resonances cause a significant rise in the harmonic levels of voltage and currents around the resonance frequency [5], [6]. Even if the capacitor bank is detuned, resonance can still be present in the distribution system owing to the capacitive nature of the load. Also, detuning is almost impossible in case of distributed capacitance throughout the distribution network. Therefore, to improve the overall power quality, it is important to classify, detect, and address different harmonic resonance scenarios in the power distribution network.

The associate editor coordinating the review of this manuscript and approving it for publication was Hiram Ponce.

TABLE 1. Comparative analysis of various techniques related to SAPF addressing harmonic resonance.

Parameters	HAPF [12]	HAPF [11]	SAPF [15]	HAPF [14]	SAPF [19]	SAPF [21]	Proposed control strategy
Overall functions performed	Resonance Damping	• Resonance Damping • Harmonic Compensation (THC)	• Resonance Damping • Harmonic Compensation (THC)	• Resonance Damping • Harmonic Compensation (THC)	• Resonance Damping • Harmonic Compensation (THC)	• Resonance Frequency detection • Resonance Damping • Harmonic Suppression (SHC)	• Resonance Frequency range detection • Resonance Damping • Harmonic Compensation (THC)
Total number of sensors required (as per single phase): PCC voltages (u_{pcc}), Source, load and filter current (i_S, i_L , i_F) and DC voltage (U_{DC}) respectively	**Two** • (u_{pcc}, i_F) - For resonance damping	**Three** • (u_{pcc}, i_F, i_S)- For harmonic compensation	**Four** • (u_{pcc})-For resonance damping • (i_F, i_L, U_{DC})- For harmonic compensation	**Three** • (u_{pcc})-For resonance damping • (i_F, U_{DC})- For harmonic compensation	**Four** • (i_S)- For resonance damping • (u_{pcc}, i_F, i_S, U_{DC})- For harmonic compensation	**Five** • (u_{pcc}, i_F, i_S)- for resonance detection • (u_{pcc})- resonance damping • (u_{pcc}, i_F, i_L, U_{DC})- For harmonic compensation	**Two** • (u_{pcc})-For resonance detection and resonance damping • (u_{pcc}, i_L)- For harmonic compensation
Additional hardware	Passive filter tuned at particular frequency	Transformer and delta connected capacitor bank are connected in series	No	L-C Passive filter tuned at particular frequency	No	External 120° square wave signal required to inject	No
Additional tasks required in the technique	• Gain adjusting circuit • Passive filter	• Passive filter	• LPF required for load voltage before harmonic detection	• Determining THD reference for low line impedance • Passive filter	None	• Determining time and amplitude of external signal injected in the circuit according to the application	• Generating database
Limitations	• Resonance frequency not detected • Assumption regarding harmonic profile of u_{pcc} • Fixed resonance frequency	• Resonance frequency not detected • Modification in conventional circuit of SAPF • Good for medium voltage application • Fixed resonance frequency	• Resonance frequency not detected • Fixed parallel and series resonance frequency • Parameter variation not discussed	Resonance frequency not detected	• Resonance frequency not detected • Deals with narrow range of frequency for resonance i.e., 211-732 Hz	• Invasive: Requires external signal injection • Involves Complex control which requires many inputs and resources • Only PFC capacitance variation is discussed	Accuracy depends on training data

There are numerous control strategies and optimization techniques for SAPF are available in literature to address different issues [7]–[10], however, very few control strategies focus on addressing harmonic resonance, especially detection of harmonic resonance. A hybrid filter with a capacitor bank in series by coupling transformer is utilized to suppress harmonic resonance in [11], providing a cost-effective solution. Another hybrid APF based on the impedance approach is proposed in [12]–[14]. A conventional control strategy for SAPF is proposed in literature which deals with resonance damping for a particular resonance frequency [15], [16]. Similarly, the concept of Resistive APF is utilized in [17] both

for resonance damping at a particular frequency and selective harmonic compensation. The possibility of unwanted amplification of the harmonics caused due to mismatch between Resistive-APF conductance and line impedance is discussed and addressed with the resonant control technique [18]. Resonance damping technique based on current source detection is proposed in [19]. However, this control technique is limited to a narrow frequency range. While most of the techniques discussed in literature focused on resonance damping, there is not much discussion regarding identification or detection of the resonance except in [20], [21]. Authors in [21] have mainly focused on the resonance in the upstream distribution network caused due to interaction between capacitor bank and source impedance. This method utilizes invasive technique of injecting external signal into the circuit to calculate power index. The disadvantage of invasive techniques is that they can compromise the distribution network performance. Also, this method requires information from four types of sensors to detect resonance frequency. Therefore, most solutions available in literature either utilise passive hybrid SAPF configuration or required additional sensors and/or hardware to address harmonic resonance. The drawback of utilising passive filters and SAPF to address harmonic resonance is that they can only address resonance in the specific frequency range and does not consider variation in system parameters.

A detailed comparison between different techniques discussed above is summarised in Table 1.

Due to continuous variation in the internal switching of capacitive equipment, there can be various possibilities in the resonance's scenarios, e.g., the level of amplification, resonance frequency and the bandwidth of the resonance. Thus, it is important to study various resonance scenarios.

Presence of resonance in the circuit usually does not create a problem as long as it is not excited. There are two types of resonance, parallel and series; both are dangerous to the power distribution network. Parallel resonance is excited by a harmonic current close to the resonance frequency, where impedance of the resonance circuit is minimum. Series resonance is excited by a harmonic voltage close to the resonance frequency, where impedance of the resonance circuit is minimum. Thus, presence of harmonic resonance is observed by measuring the impedance at the busbar or PCC in the distribution network [22]. Machine learning (ML) approach has been proposed in this paper to detect various resonance scenarios. ML has been used reliably to detect several defects, irregularities and disruptions in power grids and other issues with power quality in general [23]–[26]. Harmonic levels are amplified around resonance frequency due to presence of resonance. As a result, harmonic levels are different in presence of resonance in comparison to the case when there is no resonance. This distinction makes it a suitable problem for supervised classification ML approach. ML algorithms works by creating trained model with the help of labelled training datasets and these models are utilized in making data-driven predictions for unseen test dataset. In this paper, ML model is based on classification learning algorithms, i.e., KNN (K-Nearest neighbours) and SVM (Support Vector Machines). A classifier algorithm works by dividing data into different ''classes.'' KNN works on the principle that similar things exist in close proximity i.e., data points that are near to each other belongs to same class [27]. KNN algorithm searches for K number of nearest neighbours for given data sample and predicts class on the basis of majority labelled data sets among K nearest neighbours. In SVM, each data point is plotted in an n-dimensional space and it tries to find a hyperplane that separates the two classes [28]. The objective here is to find a plane that has the maximum margin (distance between the support vectors). Support Vectors are the points that are closer to the hyperplane and influence the position and orientation of the hyperplane. More details regarding theoretical foundation of SVM and KNN is provided in [27], [28]. This technique only requires voltage harmonics at the PCC as an input. Impedance data from the MATLAB is only required at the training stage to label dataset with corresponding resonance frequency.

Typical behaviour of the power distribution network is presented by an equivalent circuit and the load with capacitive behaviour is modelled with the help of an aggregated load. All parameters are designed on the basis of actual distribution network parameters in a way, that it has distinct resonances well below 2.5 kHz [29].

Paper is presented as follows: Section II deals with the discussion about the effect of resonance on the performance of SAPF and the methodology for the machine learning algorithm. Section III deals with the details regarding building of the realistic database with the help of an equivalent circuit and learning algorithms. Section IV presents control strategy for SAPF. Section V presents machine learning and SAPF results and section VI concludes the work. The main contribution of the paper includes: - (i) Analyse the effect of resonance on the performance of SAPF, (ii) Development of realistic database considering various system parameter variations to study resonance behaviour in power distribution network in the presence of SAPF., (iii) The formulation of a resonance detection method based on machine learning approach. (iv) Resonance detection, damping in addition to the harmonic compensation by utilising reduced number of sensors.

II. SYSTEM CONFIGURATION

Fig. 1 shows the system configuration of a simplified distribution system with SAPF and a PFC unit. Fig. 1 shows a three-phase three-wire system with source voltages, $u_{sx}(x = a, b, c)$ with line impedance of resistance R_s and inductance L_s, connected to a non-linear and linear load in parallel. Non-linear consists of an uncontrolled rectifier with an R-L load at its output terminal. The linear load consists of R-L-C parameters connected in parallel at PCC. SAPF unit contains a Voltage Source Converter (VSC) with six IGBTs and a capacitor (C_{dc}) at DC side. A coupling inductor (L_f) connects SAPF in parallel to the source and load. As shown

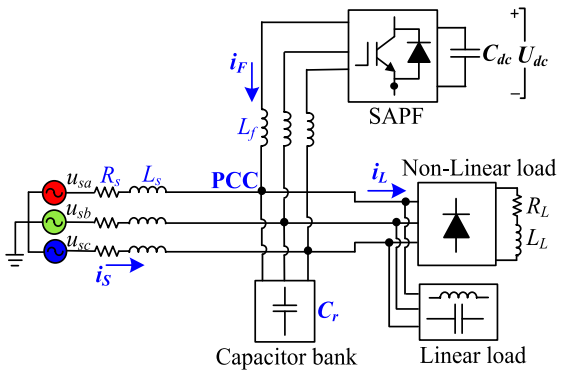

FIGURE 1. Block diagram of the distribution system with SAPF to study different resonance scenarios.

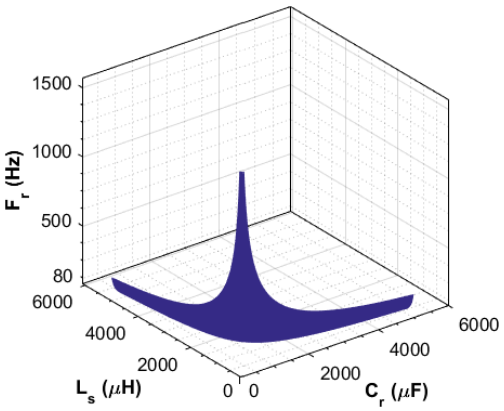

FIGURE 2. Parallel resonance caused due to interaction between capacitance of capacitor bank, (C_r) and line inductance (L_s).

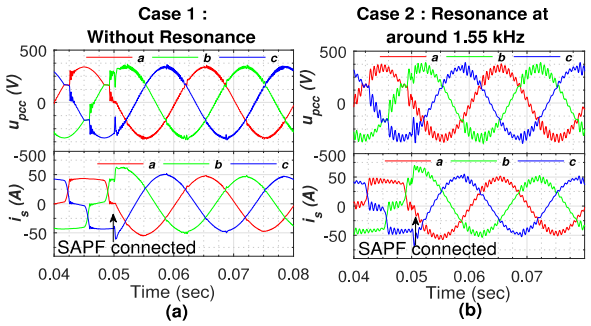

FIGURE 3. Performance of SAPF under different scenarios (a) Case 1: Without resonance, (b) Case 2: resonance at around 1.55 kHz.

in Fig. 1, a capacitor bank with capacitance C_r is connected in parallel to the source and load.

A. PARALLEL RESONANCE

Capacitor banks (see Fig. 1) are often used as a PFC unit in the distribution load and are placed near PCC. If seen from PCC towards the source, capacitor bank forms a parallel resonant circuit with the line inductance. This upstream impedance is expressed as;

$$Z_{Sr} = (Z_s || Z_{Cr}) \tag{1}$$

$$Z_{Sr} = (R_s + sL_s) \,||\, \left(1/sC_r\right) \tag{2}$$

On solving,

$$Z_{Sr} = \frac{R_s + sL_s}{1 + sC_rR_s + s^2L_sC_r} \tag{3}$$

Assuming the effect of R_s is relatively small, Eqn. (3) is simplified as:

$$Z_{Sr} \approx \frac{j2\pi fL_s}{1 + (2\pi f)^2 L_sC_r} s = j2\pi f \tag{4}$$

Now, resonance frequency from (4) is expressed as;

$$F_r \approx \frac{1}{2\pi\sqrt{L_sC_r}} \tag{5}$$

Fig. 2 shows variation in the resonance frequency (F_r) with respect to variation in both line inductance L_s and parallel capacitance C_r. Resonance frequency varies from 80 Hz toaround 1 kHz on varying L_s and C_r from the point (5000 μF, 5000 μH) to the point (100 μF, 100 μH).

B. PERFORMANCE OF SAPF UNDER RESONANCE SCENARIO

SAPF works by injecting compensating current i_{Fx} ($x = a, b, c$), at PCC to cancel out the harmonics present in source current i_{Sx}. Harmonics are injected into the source by load current i_{Lx} produced by the non-linear load. Power flow between the source and load is controlled by maintaining a constant DC voltage (U_{DC}) across the DC capacitor (C_{dc}) as shown in Fig.1. In this paper reference current for source current is generated with the help of Adaptive linear network (ADALINE) based control strategy utilising Least Mean Square (LMS) algorithm [30].

Performance of SAPF is observed for the circuit configuration shown in Fig.1 under three scenarios:

1) Case 1: Without resonance
2) Case 2: In presence of resonance of resonance at around 1550 hertz
3) Case 3; In presence of resonance at around 500 Hz

Results are presented in Fig. 3 and 4. Fig. 3 shows the performance of SAPF in the presence of resonance in terms of PCC voltages and source current for case 1 and 2. It can be observed from Fig. 3(a) and (b) that when SAPF is connected at t = 0.05 sec, compensating current (i_F) is injected into the circuit and source current (i_s) transforms into a sinusoidal waveform in phase with the PCC voltage (u_{pcc}), without any significant delay. Presence of resonance in case 2 can be observed from Fig. 3(b), which also appears in the harmonic spectra as shown in Fig. 4. Fig. 4 shows harmonic spectra of PCC voltage and the source current under three resonance conditions as explained above in case 1, 2 and 3. For case 1, there is no resonance hence THD of both PCC voltages and source current improved from 8.5 % to 3.0 % and 21.2 % to 1.97 % THD respectively as shown in Fig. 4. For case 2, there is resonance around 1550 Hz (31 harmonic order) frequency.

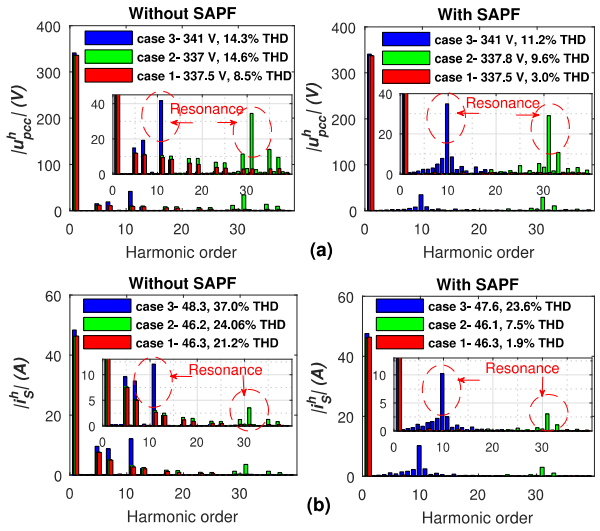

FIGURE 4. Harmonic spectra of (a) PCC voltage, $|u^h_{pcc}|$ and (b) Source current $|i^h_s|$, before and after SAPF connection under three different resonance scenarios.

THD improved from 14.6 % to 9.6 % for PCC voltage and from 24.06 % to 7.54 % for source current. It can be clearly observed that there is harmonic amplification around resonance frequency in comparison to case 1. For case 3, THD improves from 14.3 % to 11.2 % for PCC voltage and 37 % to 23.6 % THD for source current. This increase in THD is due to amplification in harmonics around the resonance frequency i.e., 500 Hz as can be clearly observed in harmonic spectra shown in Fig. 4. In both case 2 and case 3, magnitude of harmonics around resonance frequency does not reduce much even after connection of SAPF, because SAPF is only compensating harmonics injected by load with the help of compensating current. Therefore, it can be concluded that presence of resonance significantly affects overall THD of both voltages and current at PCC and hence performance of SAPF.

C. METHODOLOGY FOR CLASSIFICATION LEARNING BASED DETECTION

Different features of resonance, i.e., bandwidth, amplification ($|Z_{pcc}|/|Z_{ref}|$) and resonance frequency are shown in Fig.5 and corresponding amplification in the harmonic spectrum of PCC voltage $|u^h_{pcc}|$ and current $|i^h_s|$ is shown in Fig.4. Reference impedance (Z_{ref}) is the impedance value at the 50 Hz frequency, expressed in an extrapolated form. This distinct amplification in harmonic levels around resonance frequency compared to the case without resonance (case 1: without resonance, Fig. 4) forms the basis for the machine learning based resonance classification and detection. Since, in parallel resonance, amplification in voltage harmonic levels is more significant in comparison to the current, thus only voltage harmonic information is utilised here to detect resonance. Fig. 6 shows a methodology for classification learning based detection. Here, voltage $|u^h_{pcc}|$ spectra is required as an input being trained for respective resonance conditions with the help of learning algorithm. Simulation data, i.e., impedance at PCC, Z_{pcc} is required for labelling training data set. After training is finished with desired accuracy, unseen test data set, i.e., voltage $|u^h_{pcc}|$ harmonic spectra are subjected to the trained model for predicted result i.e., resonance frequency. Resonance is classified in terms of the frequency ranges. Thus, the bandwidth of 250 Hz is selected considering the effect in the harmonic amplification, i.e., case with resonance at 1.6 kHz frequency is labelled as "1500-1750 Hz ".

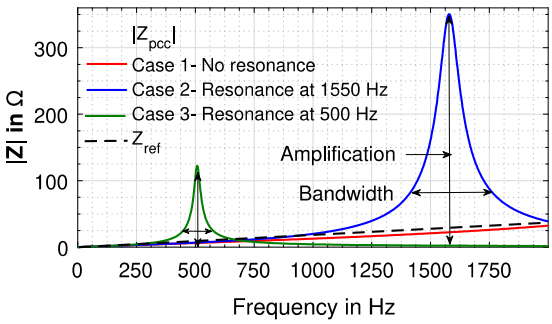

FIGURE 5. Resonance characteristics under three resonance cases: Impedance at PCC ($|Z_{pcc}|$), Reference Impedance (Z_{ref}) and bandwidth.

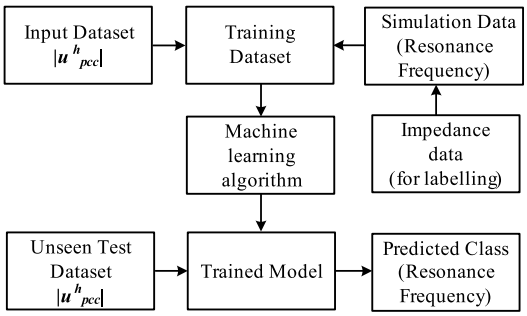

FIGURE 6. Block diagram showing the process of machine learning based resonance detection.

III. PROPOSED RESONANCE DETECTION TECHNIQUE

Three main stages for machine learning includes (a) Data generation and collection, (b) Data pre-processing, (c) Implementation of Algorithm. Fig. 1 is presented in the form of a simplified single line diagram as shown in Fig.7 (a). The network consists of mains, PCC and an R-L branch, SAPF is connected at the load end in parallel to the load and source along with a PFC unit, i.e., capacitor bank, a linear load as well as a non-linear load and harmonic current sources. Harmonic current sources consist of the harmonics injected by current source type non-linear loads. Variation in almost every parameter shown in Fig. 7 (a) is performed to build a database such that it includes all possible cases of different resonance frequencies required for training. Database building, identification and functioning of the training algorithm is discussed in the following section:

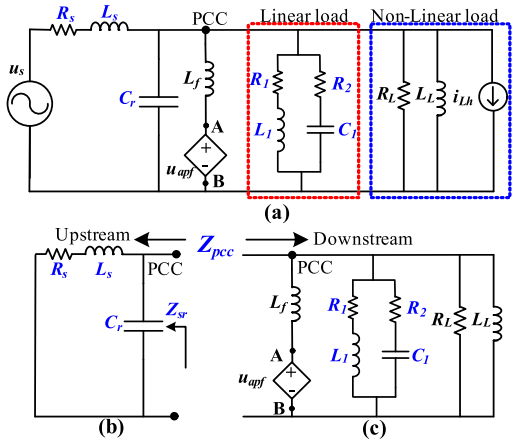

FIGURE 7. Equivalent circuit.

A. BUILDING DATABASE FOR THE LEARNING ALGORITHM

Upstream network in Fig.7 (b) consists of line impedance in parallel with shunt capacitance. The downstream network (Fig. 7(c)) consists of the load and the current harmonic emissions (i_{Lh}). Impedance Z_{pcc} represents the combined impedance of both upstream as well as downstream network. Impedance measurement at PCC ensures all parameters variations at a common point. Z_{pcc} is calculated in parts with the help of admittance Y_{pcc} as follows:

$$Y_{pcc} = Y_L + Y_{Cr} + Y_s \tag{6}$$

where $Y_{pcc} = {}^{1}/_{Z_{pcc}}$

$$Y_{pcc} = Y_{Loop} + Y_{Cr} \tag{7}$$

where $Y_{Loop} = Y_L + Y_s$ represents loop admittance, Y_L represents load admittance of the linear load as shown in Fig.7(c), Y_{Cr} represents admittance of capacitor bank and Y_s represents line admittance.

$$Y_L = \frac{1}{R_1 + jX_{L1}} + \frac{1}{R_2 - jX_{C1}} \tag{8}$$

On simplification,

$$Y_L = \frac{c + jd}{a + jb} \tag{9}$$

where, $c = R_1 + R_2$, $d = X_{L1} - X_{C1}$, $a = R_1R_2 + X_{L1}X_{C1}$ and $b{=}(R_2X_{L1} - R_1X_{C1})$

Now, loop admittance Y_{Loop} is calculated as;

$$Y_{Loop} = Y_L + Y_s \tag{10}$$

$$Y_{Loop} = \frac{c + jd}{a + jb} + \frac{1}{R_s + jX_{Ls}} \tag{11}$$

$$Y_{Loop} = \frac{a + cR_s - dX_{Ls} + j(b + cX_{Ls} + dR_s)}{aR_s - bX_{Ls} + j(bR_s + aX_{Ls})} \tag{12}$$

$$Z_{pcc} = \frac{1}{Z_{Loop}} + \frac{1}{Z_{Cr}} \tag{13}$$

where, $Z_{Cr} = -({}^{1}/_{X_{Cr}})$ and $Z_{Loop}{=}({}^{1}/_{Y_{Loop}})$, on substituting values of Z_{Cr} and Z_{Loop} in (17).

$$Z_{pcc} = \frac{p + iq}{r + js} \tag{14}$$

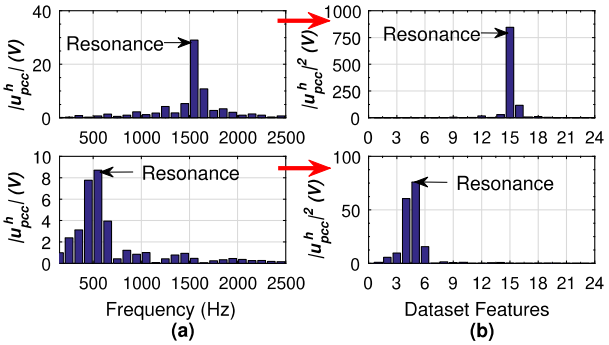

FIGURE 8. Dataset consisting of voltage and current harmonic spectra for specific resonance case scenario of 1.55 kHz.

where,

$$p = X_{Cr}\left[(R_1R_2 + X_{L1}X_{C1})R_s - (R_2X_{L1} - R_1X_{C1})X_{Ls}\right]$$

$$q = X_{Cr}\left[(R_2X_{L1} - R_1X_{C1})R_sX_{Cr} + (R_1R_2 + X_{L1}X_{C1})X_{Ls}X_{Cr}\right]$$

$$\begin{aligned} r &= (R_1R_2 + X_{L1}X_{C1})(X_{Cr} - X_{Ls}) - (R_2X_{L1} - R_1X_{C1})R_s \\ &\quad + (R_1 + R_2)R_sX_{Cr} - (X_{L1} - X_{C1})X_{Ls}X_{Cr} \\ s &= (R_2X_{L1} - R_1X_{C1})(X_{Cr} - X_{Ls}) + (R_1R_2 + X_{L1}X_{C1})R_s \\ &\quad + \left[(R_1 + R_2)X_{Ls} + (X_{L1} - X_{C1})R_s\right]X_{Cr} \end{aligned}$$

Total impedance calculated at PCC is utilised to observe different resonance scenarios on varying load and source parameters. The main reason behind resonance is the capacitive behaviour of the load. Therefore, effect of the inductive non-linear load is taken as harmonic current emissions as shown in Fig. 8, and instead of R-L parameters, R-L-C aggregated load is considered to represent load impedance for observing resonance behaviour with the help of total impedance Z_{pcc} as shown in Fig.8(c). Now, considering non-linear R-L parameters, total load admittance Y_{Leq} is calculated as:

$$Y_{Leq} = Y_L + Y_{R_L} + Y_{L_L} \tag{15}$$

$$Y_{Leq} = \frac{c + jd}{a + jb} + \frac{1}{R_L} + \frac{1}{jX_{L_L}} \tag{16}$$

Applying KCL at PCC in Fig. 8(a): Voltage at PCC is expressed as:

$$u_{pcc} = \frac{u_{apf}Z_sZ_{C_r}Z_{Leq} + u_sZ_fZ_{C_r}Z_{Leq} - I_{Lh}Z_fZ_sZ_{Leq}Z_{C_r}}{Z_sZ_{C_r}\left(Z_{Leq} + Z_f\right) + Z_fZ_{Leq}\left(Z_{C_r} + Z_s\right)} \tag{17}$$

Therefore, harmonic spectrum components voltage at PCC in magnitude form is calculated for various conditions in order to form database. Since, database consists of various datasets, each consisting harmonic spectrum of voltage at PCC. Fig.8 (a) shows magnitude of harmonic spectrum for two different resonance scenarios i.e., for 500 and 1550 Hz considering one household and base parameter values as shown in Table 2. Since there are many other possible resonance scenarios possible with different amplification factor,

TABLE 2. Base values.

Parameters	C_r (μF)	L_s (μH)	R_1 (Ω)	R_2 (Ω)	L_1 (mH)	C_1 (μF)
Values	10	1000	50	15	10	1

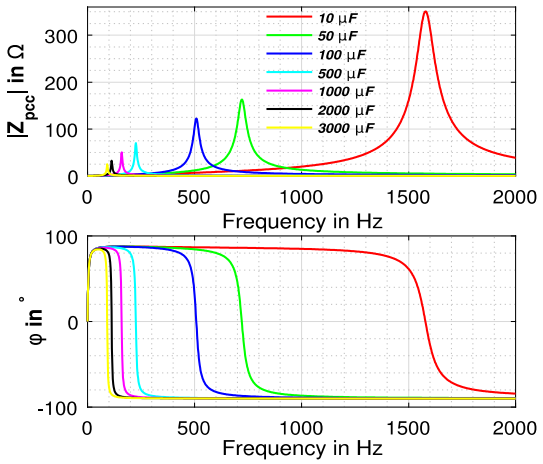

FIGURE 9. Variation in resonance frequency for different capacitance C_r values considering all other circuit parameters constant.

thus final dataset is obtained by considering square of values shown in Fig 8(b). Fig. 8(b) shows datasets for different resonance scenarios each with different resonance frequency as well as magnitude. On comparing harmonic spectrum shown in Fig. 8(a) and 8(b), datasets component in Fig. 8(b) are more distinctive with respect to the harmonic component around resonance frequency.

Effect of parameter variation is observed and discussed below by keeping other parameter values fixed, as shown in Table 2.

1) VARIATION IN PARALLEL CAPACITANCE, C_r

Fig. 9 shows variation in total impedance at PCC calculated for different values of parallel capacitance, C_r. Resonance frequency decreases from 1.6 kHz to 0.1 kHz with the decrease in the amplification factor on increasing capacitance value from 10 μF to 3000 μF. The corresponding change in phase of the harmonic impedance show transition from the inductive to the capacitive behaviour

2) VARIATION IN LINE INDUCTANCE, L_S

Variation in total impedance Z_{pcc} for different values of line inductance L_s is shown in Fig. 10. Resonance frequency decreases from 1.75 kHz to 0.9 kHz with decreases in amplification factor on increasing line inductance L_s from 800 μH to 3000 μH.

3) VARIATION IN LOAD IMPEDANCE

Fig. 11 shows the variation in the parameters of the aggregated load indirectly by varying number of households. Based on various resonance cases, as shown above, ranges of all parameters are selected for training data formation, shown

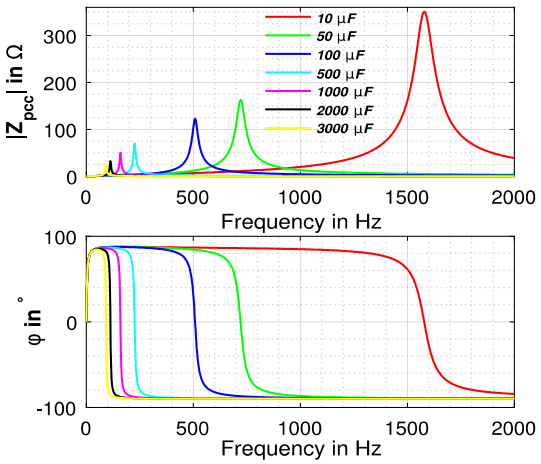

FIGURE 10. Variation in resonance frequency for different values of line impedances L_S considering all other circuit parameters constant.

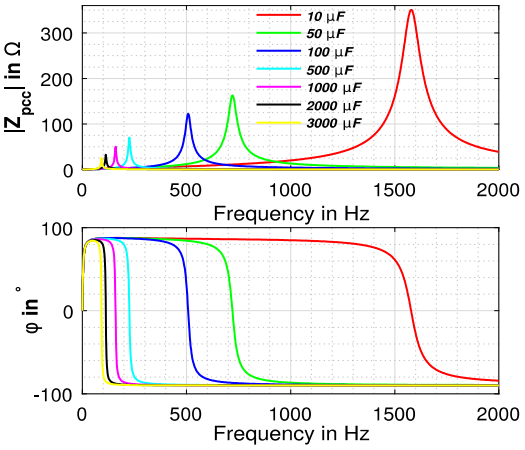

FIGURE 11. Impedance obtained after variation in the number of households (n_h) from 30 to 250.

TABLE 3. Parameter values.

Parameters	Value Range
C_r (μF)	10 – 3000
L_s (μH)	100 – 3000
R_1 (Ω)	10 –300
R_2 (Ω)	5 – 100
L_1 (mH)	0.5 – 100
C_1 (μF)	0.1 – 100
n_h	30 – 250

in Table 3. Total load impedance is varied by varying the number of households, values shown in Fig.9 and 10 are for one household load. For clarity, variation in number of households is shown for one particular value of Shunt capacitance, $C_r = 200\mu F$, with other parameters values fixed as shown in Table 2. Resonance frequency increases from 500 Hz to 1.8 kHz with the decrease in amplification factor on increasing number of households from 30 to 250 as shown in Fig.11. Corresponding variation in phase is also shown in Fig. 11.

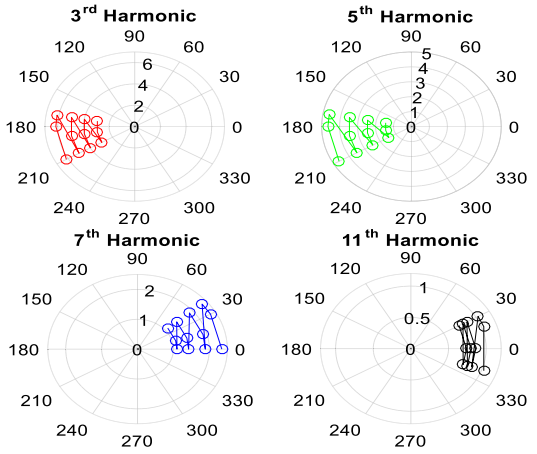

FIGURE 12. Source voltage distortion for different harmonic orders.

4) SOURCE VOLTAGE DISTORTIONS

Variation in source voltage (u_s) distortion is done by varying magnitude and angle within a range as shown in Fig. 12. Total 12 variations for 3rd, 5th, 7th and 11th harmonics are considered to build the database as shown in Fig. 12.

5) CURRENT EMISSIONS

Current harmonics are injected from the non-linear load. Therefore, variation in current harmonics is mostly governed by variation in the load parameters.

B. ITERATIVE INCREASE IN THE DATABASE POPULATION

To create a realistic database, datasets are identified, selected and artificially increased. The process for determining database for training and testing is explained below.

Based on total and reference impedance obtained after variation of all parameters as discussed earlier. Cases with amplification factor ($|Z_{pcc}|/|Z_{ref}|$) smaller than 1 are considered as cases without resonance and cases with amplification factor greater than 10 are not considered in database. Cases with resonance frequency outside the range 0-2.5 kHz are considered as cases without resonance labelled as "No Resonance."

Fig. 13 shows the process for iteratively increasing the database on the basis of variations in the equivalent circuit parameters. Based on the variations in different parameters such as voltage distortion, line impedance, PFC capacitance, number of households, and load parameters, different resonance scenarios are generated. All cases generated by individual parameters variations are discussed and presented earlier in this section.

1) DATABASE DETAILS GENERATED FOR TRAINING AND TESTING

The database is generated in an iterative manner i.e., increasing the size, taking into account one parameter at a time as shown in Fig. 13. Details regarding total number of cases for each parameter is presented in Table 4 and Fig.13. Among ten variations in load parameters, half values are considered for testing and the remaining half are considered for testing to separate database.

TABLE 4. Training and testing database.

Database	Complete Data	Training Data	Testing Data
Total number of cases with resonance in 0-2.5 kHz	88233	45810	42423
Cases without resonance	55767	26190	29577
Total number of cases	12*10*10*12 *10= 144000	12*10*10*12 *5= 72000	12*10*10*12 *5= 72000

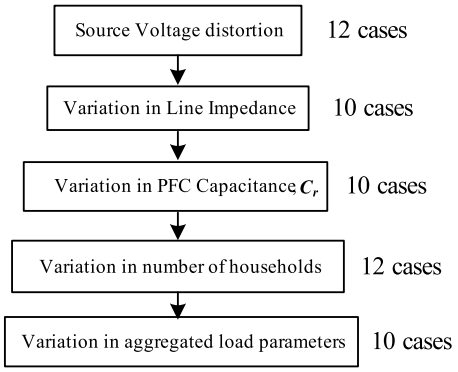

FIGURE 13. Iterative increase in the database.

C. CLASSIFICATION LEARNING ALGORITHMS

Simulations are carried out to build a database consisting of all possibilities associated with different characteristics of harmonic resonance such as resonance frequency, amplification factor and bandwidth. Classification learning app toolbox available in the MATLAB is utilized to perform various operations associated with training, and the database is tested for multiple algorithms. Algorithm corresponding to the trained model with the highest accuracy is selected for resonance detection.

Among various learning techniques available in the literature, KNN and SVM techniques are observed to provide the best performance in terms of accuracy. The working of both algorithms is shown in Fig. 14. Initial three steps are the same for both SVM and KNN, as shown in Fig.14.

Data pre-processing is required to extract only the magnitude of the voltage harmonics samples in per unit. Feature extraction involves only selecting the particular range of harmonics for the training purpose, only harmonics from 0 to 2.5 kHz are considered. Normalization of the input samples ensures that both components with a large and small range have equal weightage in the training process. Further distinct steps for both algorithms are explained as follows:

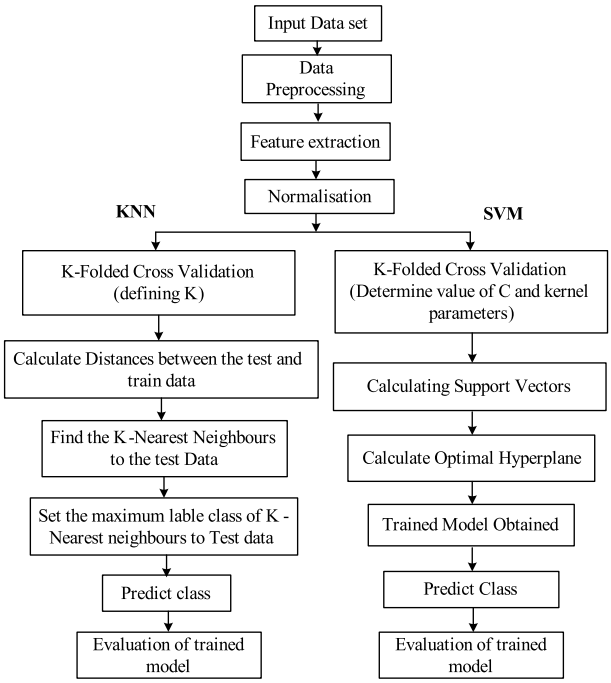

FIGURE 14. Working of both SVM and KNN algorithm.

1) KNN-K NEAREST NEIGHBOURS

KNN works by calculating the distance between training and test data [27], [31]. Nearest neighbours are selected with the help of the closest distance. K in KNN stands for the number of nearest neighbours considered to predict the class of the unseen test data. The value of K and the distance metric settings are decided such that optimum performance is achieved. Here, the number of input samples (i.e., labelled data samples), n is large; therefore, K is decided with the help of cross-validation (CV). In CV, input data samples are arbitrarily divided into train and test data continuously till each data sample is used as test data. Accuracy of the model is checked against CV-data for random K values. The model for which the best accuracy is obtained is considered as the best K value. Here, maximum accuracy for CV datasets is observed at K = 15. For distance metric all distance metrics are evaluated to achieve best accuracy. Table 5 shows accuracy corresponding to different distance metric in KNN, both Euclidean and Cosine methods have similar performance.

If $x_i(i = 1, 2, 3 \ldots, n)$ and $x_t(t = 1, 2, 3 \ldots, n)$ represents train and test data respectively with p number of features, then distance metric (d) between test and training data is defined as:

$$d(x_i, x_t) = \sqrt{(x_{i1} - x_{t1})^2 + (x_{i2} - x_{t2})^2 + \ldots (x_{ip} - x_{tp})^2} \quad x_i \in x_{i1}, x_{i2}, x_{i3}, \ldots\ldots\ldots x_{ip} \tag{18}$$

where $x_{i1} = \left|u_{pcc}^{3h}\right|, x_{i2} = \left|u_{pcc}^{5h}\right|, \ldots\ldots x_{i24} = \left|u_{pcc}^{49h}\right|$

Therefore, $p = 24$ (number of features in one data sample)

Here $n = 72000$ (See Table 4)

After calculating distance (d) as shown in Fig 15, K nearest neighbours are identified. At the final stage, test data is predicted with the same class as the most common labelled class among K nearest neighbours.

2) SVM-SUPPORT VECTOR MACHINES

SVM works by creating a hyperplane to separate various classes of the input data set [28]. It has many features to deal with extensive data with overlapping and noise such as creating hyperplane in higher dimensional space, ignoring outliers, kernel tricks etc. This hyperplane is achieved with the help of a decision function $f(x)$ as follows:

$$f(x) = sign(g(x)) \tag{19}$$

$g(x)$ is derived with the help of input training vectors x_i and classes Y, where $Y = (y_1, y_2, \ldots y_c), y \in [-1, 1]$, c is the number of labelled classes.

$$g(x) = (w.x) + b \tag{20}$$

w and b are selected such that hyperplane is created to classify testing data correctly by ensuring distance between the hyperplane, and closest vectors is maximum, this constraint is expressed as:

$$y_i((w, x_i) + b)) \geq 1 - \xi_i\{\xi_i \geq 0, \textit{ for all } i\} \tag{21}$$

Maximizing the margin between two classes is solved as an optimization problem:

$$\Phi(w, \xi) = \min\left\{\left(\frac{1}{2}\right)\|w\|^2 + C\sum_{i=1}^{n}\xi_i\right\} \tag{22}$$

C is a regularization parameter. Eqn. (22) is solved with the help of Lagrange multipliers and is simplified by the dual formulation of the problem. After applying computational techniques and certain simplification, consequently $g(x)$ is expressed as:

$$g(x) = \sum_{i=1}^{N}\alpha_i y_i\langle x, x_i\rangle + b \tag{23}$$

In (23), x is a test vector, N is the number of support vectors, and α is Lagrange multiplier. Also, for large and complex data, which is not easily linearly separable as is the case discussed in this paper, kernel function K is used. K can be of different types and is preselected with cross-validation, as shown in Fig. 14. A thorough discussion about SVM fundamentals and detailed derivation is available in the literature [23], [32].

Above operations are performed with the help of SVM library available in MATLAB. Inputs such as C, kernel parameters values are required to calculate support vectors and these are decided with the help of CV. The C parameter adds penalty for each misclassified data point. Different random values of C are validated with CV datasets and this exercise is repeated for multiple times on various CV datasets. The model for which best accuracy is obtained, C value

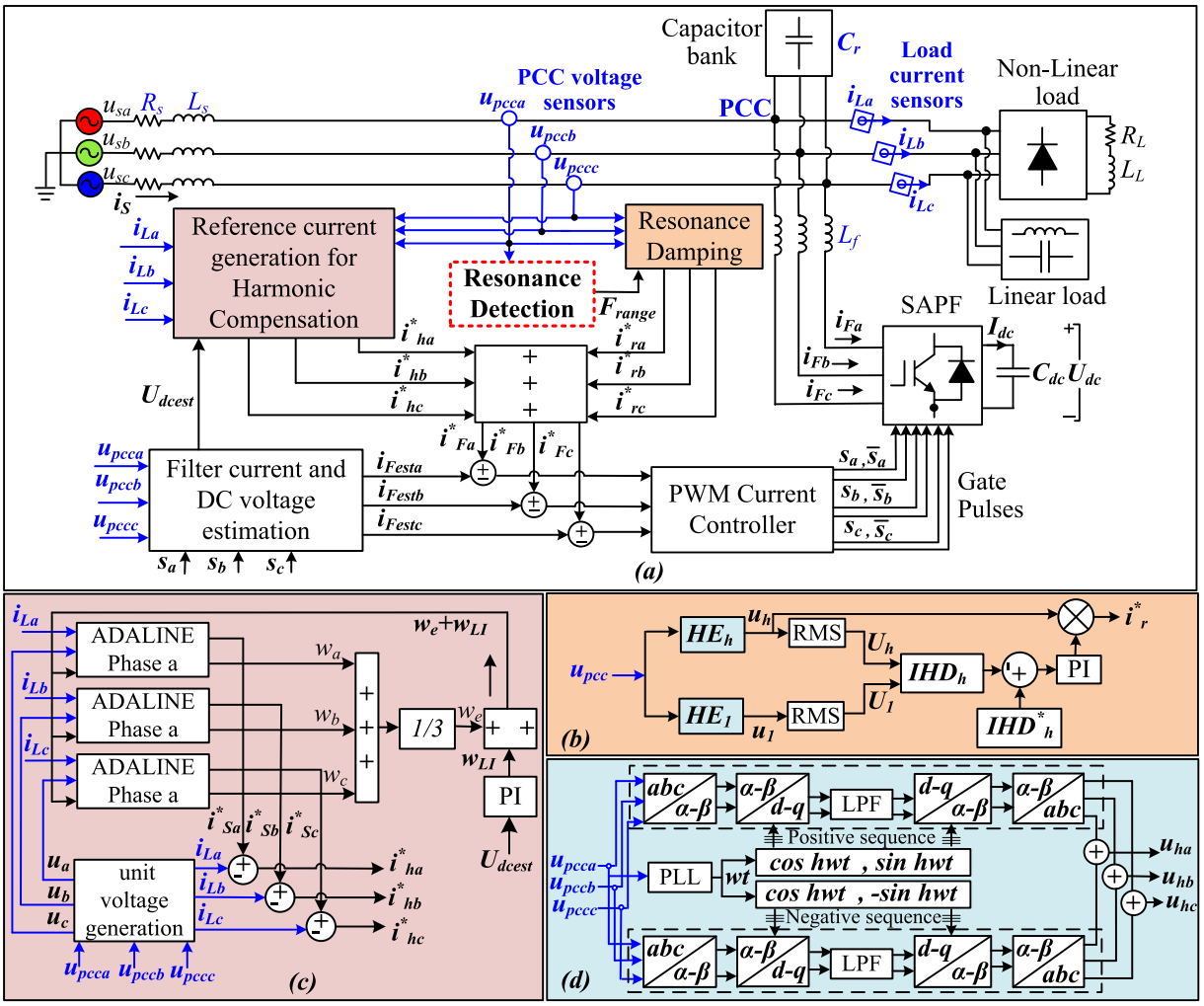

FIGURE 15. SAPF operation in Harmonic Compensation and resonance damping mode: (a) Block diagram of detailed SAPF circuit, (b) Reference current generation technique for harmonic compensation, (c) Reference current for resonance damping, (d) Harmonic extraction (HE) from PCC voltages.

corresponding to that model is selected for testing. This process is also called randomized search with cross validation score. $C = 100$ is selected for accuracy of 98.5 %. For kernel, cubic function is selected after evaluating multiple kernel function. Table 5 shows accuracy corresponding to different kernel functions in SVM against test data. Optimal hyperplane (23) is defined with the help of support vector, and test data samples are classified accordingly. Performance of the trained model is evaluated with the help of accuracy of the predicted class.

IV. CONTROL STRATEGY FOR SAPF OPERATION

Control strategy for SAPF to address to perform both harmonic compensation as well as resonance damping is discussed in this section. Complete operation of SAPF in presented in detail in Fig.15. As shown in Fig. 15(a), resonance detection takes place with by sensing voltage at PCC explained in earlier section. With the help of resonance frequency, reference current for damping is generated as shown in Fig. 15(b) which adds up in the reference current generated for harmonic compensation as shown in Fig. 15(c). Here, Reference current generation technique (RCGT) for harmonic compensation only senses load current and PCC voltages sensors as shown in Fig. 15 (c). DC voltage is estimated in order to reduce sensor required for sensing actual DC voltage in power flow control. DC voltage is estimated with the help of MRAS technique discussed in detail in [33]. The technique utilized for Harmonic extraction is shown in Fig. 15(d). Detailed procedure is expressed as follows:

A. REFERENCE CURRENT GENERATION TECHNIQUE

RCGT is developed with the help of Adaline based LMS algorithm. Also, detailed control strategy is provided in reference [30], [33], [34]

LMS algorithm works by calculating weights (w) such that mean square error between desired and actual quantity is minimum. Corresponding weight update equation for each

phase at k^{th} instant is expressed as:

$$w_x(k+1) = w_x(k) + \eta\{i_{Lx}(k) - w_x(k)\,u_x(k)\}\,u_x, x\epsilon a, b, c \quad (24)$$

where $\eta(0 < \eta < 1)$ is converging coefficient. u_x are unit vector voltages calculated by expressing voltage at the PCC in per unit. Weights are calculated for each phase separately and equivalent weight (w_e) is calculated by taking average of three weights as shown in Fig. 15(b). Reference current (i^*_{Sx}) is calculated as follows;

$$i^*_{Sx} = (w_e + w_{LI}) * u_x \quad (25)$$

w_{LI} is loss component of current obtained from DC voltage controller utilized to maintain DC voltage constant at reference value, i.e., U^*_{DC} (700 V).

$$U_e(k) = U^*_{DC}(k) - U_{DCest}(k) \quad (26)$$

$$w_{dc}(k+1) = w_{dc}(k) + k_{id} * \{U_e(k+1) - U_e(k)\} + k_{pd} * U_e(k+1) \quad (27)$$

where, U_e is error between actual and reference DC voltage U^*_{DC}. k_{pd} and k_{id} are proportional and integral gains of the PI controller. Reference harmonic compensation current, i^*_{hx} is generated by subtracting actual load current i_{Lx} from sinusoidal reference current i^*_{Sx} as shown in Fig. 15(c).

B. RESONANCE DAMPING TECHNIQUE

According to detected resonance frequency range (F_{range}), corresponding harmonic component (u_h) and fundamental component (u_1) of PCC voltage is extracted as shown in Fig.15(b). With the help of extracted components IHD (Individual Harmonic Distortion) with respect to harmonic order around resonance frequency (h) is calculated as:

$$IHD_h = \frac{U_h}{U_1} \quad (28)$$

where, U_h and U_1 represents RMS value of harmonic order $'h'$ and fundamental component of PCC voltage respectively. IHD^*_h is 3%, standard limit for individual harmonic distortion for voltages according to IEEE standard 519 [35]. The difference between standard and obtained IHD is sent to PI controller in order to regulate actual distortion limits. Thus, reference current for damping resonance is obtained as follows:

$$i^*_r = \left(IHD^*_h - IHD_h\right)\left(k_p + {}^{k_i}/_{s}\right) * u_h \quad (29)$$

Here, it is to be noted that, here only one harmonic order is taken into account. According to predicted frequency range, multiple harmonic orders within frequency range can be taken and reference current is calculated for each order in similar manner. Total reference current for damping is expressed as:

$$i^*_r = \sum_h i^*_{rh} \quad (30)$$

Thus, reference current in (30) includes all harmonic orders within resonance frequency range. Similarly, for multiple resonance cases, all such reference components for different harmonic order can be added together to obtain total reference current. Here, extracting total harmonic component of voltage (u_{pcc}) is avoided as tracking high order damping reference current is difficult considering fixed switching frequency.

1) HARMONIC EXTRACTION (*HE*)

Three phase PCC voltages are transformed into $d-q$ coordinates with the help of unit vector generated with the help of PLL. In order to extract particular order harmonic (h), rotating frequency of unit vectors is set accordingly i.e., $'h'$ times of the line frequency. DC component is extracted from transformed vectors with the help of LPF of cut off frequency 1 Hz. Using inverse transformation, extracted component in $d-q$ frame is transformed into three phase positive sequence component. Corresponding negative sequence component can be obtained in a similar way by using unit vector rotating in opposite direction as shown in Fig.15(d).

2) HARMONIC COMPENSATION AND RESONANCE DAMPING REFERENCE CURRENT GENERATION

Total reference current is obtained by adding both reference harmonic current i^*_h as shown in Fig. 15(b) and reference damping current i^*_r as shown in Fig.15(c).

$$i^*_{Fx} = i^*_{hx} + i^*_{rx} x\epsilon a, b, c \quad (31)$$

Reference filter current and actual filter current are sent to PWM current controller to generate pulses for VSC as shown in Fig. 15(a). Here, in place of actual filter current, estimated filter current is utilised to reduce the number of current sensors. Filter current is calculated with the help of switching states and inverter output voltages.

$$i_{Festx} = \frac{1}{L_f}\left\{\int \left(u_{pccx} - u_{xn-est}\right)\right\} \text{x}\epsilon\text{a, b, c} \quad (32)$$

where, v_{xn-est} is inverter output voltage, v_{an-est}

$$u_{an-est} = \left[U^*_{DC}(k) - U_e(k)\right] * \left[\frac{2}{3}S_a - \frac{1}{3}S_b - \frac{1}{3}S_c\right] \quad (33)$$

where, U_e is error between U^*_{DC} and U_{DCest}. Similarly, u_{an} and u_{bn} can also be estimated. Detailed derivation is provided in [33].

V. RESULTS AND DISCUSSION

Performance of SAPF is evaluated in three modes. Mode I: Resonance detection, Mode II: Harmonic compensation, Mode III: Harmonic compensation and Resonance damping.

A. MODE I: RESONANCE DETECTION

For resonance detection, the number of datasets produced for both training and testing is shown in Table 4. As shown in Table 4, out of 144000 datasets, there are 61 % cases with resonance within 0-2.5 kHz and 38 % cases without resonance. Each dataset includes a set of voltage harmonic

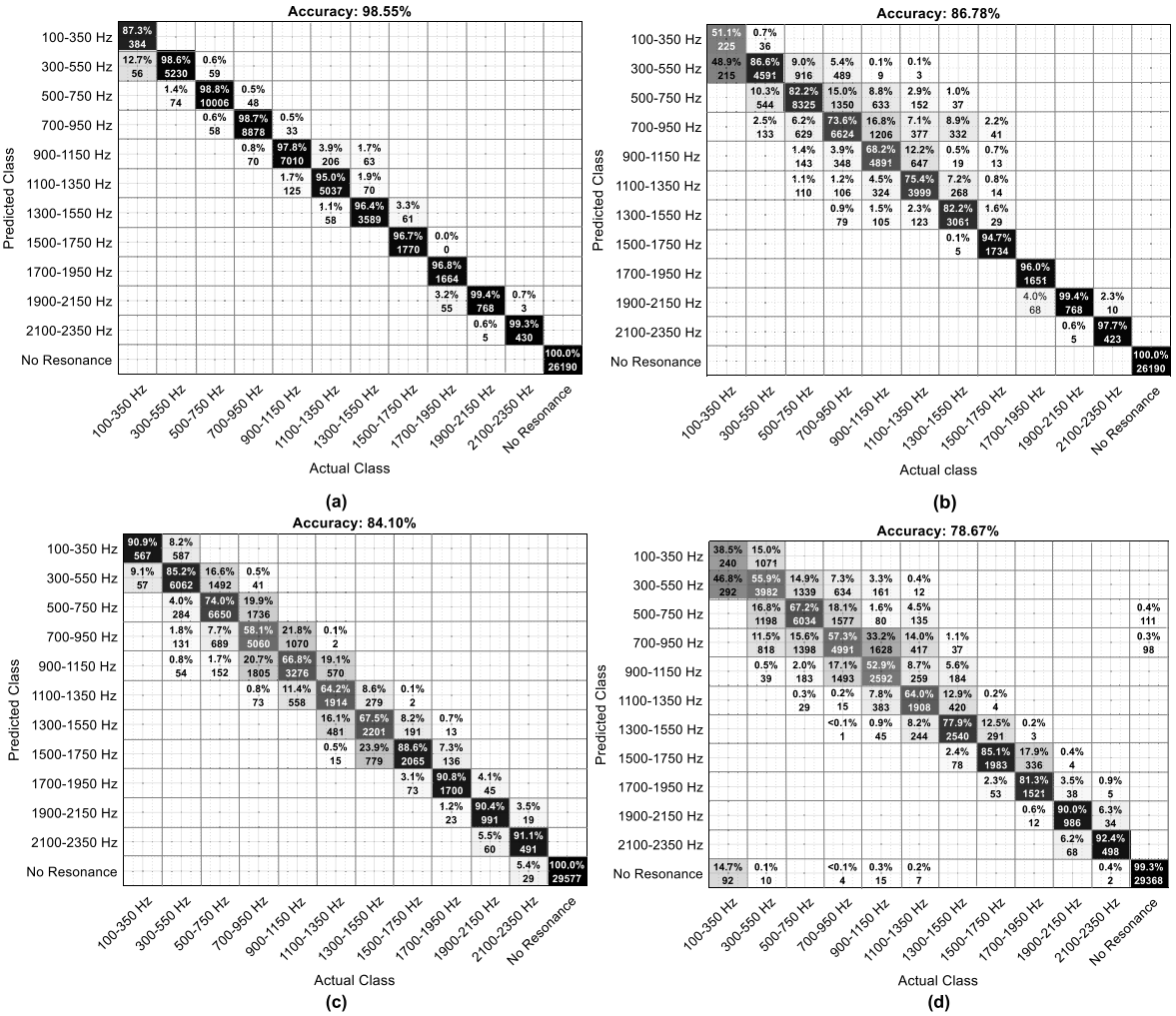

FIGURE 16. Confusion Matrices: (a) Confusion matrix for trained model by SVM, (b) Confusion matrix for trained model by KNN, (c) Confusion matrix for test data prediction by SVM, (d) Confusion matrix for test data prediction by KNN.

spectra in the range of 0-2.5 kHz. Training and testing data are generated by considering different values of load parameters and the number of households. Now, to label each dataset, the following points are selected. (1). Cases without any resonance: Such datasets include cases without any resonance within 0-2.5 kHz or amplification factor less than 1. Such datasets are labelled as "No Resonance." (2). Cases with resonance: Such datasets include cases with resonance frequency within 0-2.5 kHz. On the basis of the peak in the impedance, i.e., at resonance frequency, amplification of harmonics is generally spread around 200-300 Hz range (see Fig.5). Thus, taking into account bandwidth of the resonance, datasets are labelled in terms of the frequency range. e.g., dataset belonging to 1650 Hz resonance frequency, is labelled as "1500-1750 Hz" frequency range.

1) PERFORMANCE OF CLASSIFICATION LEARNING ALGORITHM FOR TRAINING DATA

Training data consists of the data labelled with respect to the class it is associated with. Now, data is trained by SVM and KNN algorithm with respect to the corresponding labelled class. At the training stage, algorithms learn from the labels provided as an input to algorithm and then performs the classification as discussed earlier.

The performance of both classifiers SVM and KNN is measured with the help of the Confusion Matrix. Confusion matrix shows actual classes along columns and corresponding predicted classes along rows as shown in Fig. 16. Confusion matrix effectively showcases the performance of the model in detail. In addition to overall accuracy of the trained model, confusion matrix also shows prediction accuracy with respect to each class (different frequency ranges).

Overall accuracy of the ML model is defined as total number correctly predicted cases out of all cases. For individual cases, performance parameters like precision and recall can easily be calculated for each class with the help of confusion matrix. Precision is defined as the number of correctly predicted cases of class A out of all predicted cases in class A. Similarly, recall is total number of correctly predicted cases of class A out of actual number of cases in class A, where

A represents each class shown in confusion matrix. For example, precision and recall for class ''300-550 Hz'' from confusion matrix shown in Fig. 16(a) is calculated as follows:

$$Precision = \left\{\frac{5230}{56+5230+59}\right\} * 100 = 97.84 \quad (34)$$

$$Recall = \left\{\frac{5230}{5230+74}\right\} * 100 = 98.604 \quad (35)$$

Accuracy of the trained model by SVM and KNN is 98.55% and 86.78 % respectively, as shown in Fig. 16 (a) and (b). Considering the case of 100-350 Hz range in confusion matrix shown in Fig.16 (a), 12.7 % of datasets with actual resonance frequency range in 100-350 Hz is falling in 300-550 Hz range, which is true for some instances, as there is 50 Hz overlap and cases with resonance frequency between 300-350 Hz can be classified as in both categories. Similarly, for KNN, 48.9 % of datasets with actual resonance frequency in 100-350 Hz is falling in 300-550 Hz range as shown in Fig. 16(b). It is to be noted here that classification of cases without resonance is attained with 100 % accuracy by both KNN and SVM as shown in Fig. 16 (a) and (b). It can be observed from confusion matrix in Fig. 16 (a-b) that, accuracy for the datasets in higher resonance frequency range is greater than in lower frequency range, which shows that most cases with higher resonance frequency also have relatively higher amplification factor.

Due to the considerable difference in the trained model's accuracy by both KNN and SVM algorithms, a trade-off between computation time and accuracy is made according to the requirements. Table 5 shows corresponding computation time and accuracy of both SVM and KNN algorithms. The SVM algorithm performs better in terms of accuracy than KNN with more than 90 % accuracy, i.e., 98.55 % and 95.6 % with cubic and Gaussian kernel function, respectively. KNN algorithm with the Cosine distance metric consumes less training time, i.e., 99 secs, which is much lesser than SVM. Therefore, considering the slow speed of SVM, KNN with 86.78 % accuracy and fast speed is preferred for training.

2) PERFORMANCE OF CLASSIFICATION LEARNING ALGORITHM FOR UNSEEN TEST DATA

Performance of trained model obtained by SVM Cubic (maximum accuracy) and Cosine KNN (minimum training time) is observed by subjecting it with the unseen test data. The trained model with 98.55 % (Fig. 16 (a)) accuracy is tested against new unseen data and predicted class is shown with the confusion matrix in Fig. 16(c). As shown in Fig. 16(c), the prediction accuracy obtained from SVM is 84.1%.

It can be observed from Fig. 16(c) that prediction accuracy for cases without resonance, and for cases with higher resonance frequency is 100 % and ∼90 % respectively. Similarly, the accuracy of the trained model by KNN, when subjected to test data is 78.67 %, as shown in Fig. 19. Here, the accuracy of predicted class for ''No resonance'' cases is 99.3 %, with only 0.7 % falling into ''500-750 Hz'' and ''700-950 Hz'' class.

TABLE 5. Accuracy and computation time.

Classifier		Accuracy (%)	Predicted Speed (obs/sec)	Training Time (sec)
Preset	Kernel Function / Distance Metric			
Cubic SVM	Cubic	98.55	∼2400	40758
Fine Gaussian SVM	Gaussian	95.6	∼430	22998
Medium KNN	Euclidean	86	∼1500	116.56
Cosine KNN	Cosine	86.78	∼1700	99.133
Cubic KNN	Minkowski (Cubic)	84.5	∼46	3162.8

From the confusion matrix shown in Fig.16(c) and (d), it can be found that there is an overlap of 50 Hz in various classes (resonance frequency ranges). Due to this most of the false prediction falls into the nearest range of resonance class. E.g., out of 624 datasets (240+292+92) belonging to ''100-350 Hz'' class in confusion matrix shown in Fig.16(d), 38.5 % of datasets show true prediction while 61.5 (46.8+14.7) % of datasets show false prediction identified as ''300-550 Hz'' and ''No Resonance,'' respectively. Here, cases with resonance frequency in ''300-350 Hz'' range will fall in both ''100-350 Hz'' and ''300-350 Hz'' class.

B. PERFORMANCE OF SAPF FOR COMPENSATING HARMONICS AND RESONANCE DAMPING

Performance of SAPF under two different resonance cases is shown in Fig. 17 in terms of PCC voltage, source current, compensating current and FFT analysis. In Fig 17(a), SAPF is connected at t = 0.05 sec improving waveforms of PCC voltages and source current from distorted waveforms to sinusoidal. At this instant (t = 0.05-0.08), SAPF only operates in Mode II (Harmonic compensation), thus harmonics amplified due to resonance still appears in both PCC voltage and source current waveform. At t = 0.08, SAPF starts operating in Mode III, thus adding resonance damping component in compensating current which improves THD of both PCC voltage and source current from 14.6 % to 3.52 % and 24.06% to 3.12% respectively as shown in Fig. 17(b). Similarly for case 3, harmonics are considerably reduced when SAPF operates in Mode III at t = 0.08 sec in comparison to Mode II improving THD of PCC voltage and source current from 14.3% to 3.33 % and 37 % to 4.87% respectively as shown in Fig. 17(d). Corresponding FFT analysis is shown in Fig. this and this. Also, IHD of 31st and 10th harmonic in PCC voltage for case 2 and 3 improved from 5% to 1.9 % and 12.2 % to 2.2 % respectively after resonance damping.

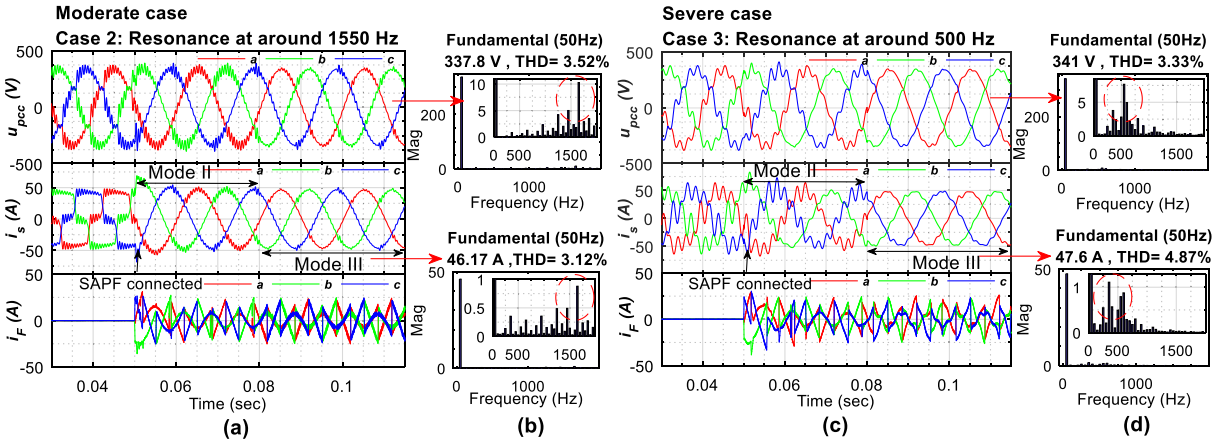

FIGURE 17. Performance of SAPF under different operating modes in terms of PCC voltages (u_{pcc}), Source currents (i_S), Filter currents (i_F): (a) Case 2: Resonance at around 1550 Hz, (b) FFT analysis, (c) Case 3: Resonance at around 500 Hz, (d) FFT Analysis.

Also, estimated quantities i.e., filter current and DC voltage are shown in Fig. 18. These estimated quantities are utilised in control algorithm to reduce the requirement of actual sensors.

C. PERFORMANCE OF PROPOSED TECHNIQUE IN PRESENCE OF NOISE

Performance of SAPF is tested in presence of noise in both voltage and current measurement. Effect of noise is analysed at two stages of the proposed work stated as follows:

1) EFFECT OF NOISE ON PERFORMANCE OF ML MODEL FOR HARMONIC RESONANCE DETECTION

Resonance detection only requires voltage harmonic data as an input. Therefore, noise is added in voltage harmonic data to evaluate performance of the trained model. An example showing difference between harmonic profile of voltage with and without noise is shown with the help of FFT analysis in Fig. 19. Presence of noise can be observed from increased voltage harmonic levels around 1500 Hz shown in Fig 19 (b). Now, previously trained SVM model shown in Fig. 16(a) is utilized for testing i.e., ML model is trained with the samples that do not contain noise. It is to be noted that a pre-trained ML model is used for testing, thus prediction of resonance does not take additional time in the control unit. From unseen test data, noise is added in 25 % of test datasets i.e., from total of 72000 samples (Table 4), noise is added in 18000 samples.

Performance of trained model obtained by SVM is observed by subjecting it with unseen test data containing noise. Predicted class is shown with help of confusion matrix in Fig.20. The prediction accuracy obtained from SVM trained model is 80.24 % as shown in Fig.20. It can be observed from Fig. 20 that prediction accuracy for cases without resonance, and for cases with higher resonance frequency is 99.4 % and ∼85-90 % respectively. This is due to high magnification ratio at higher frequency ranges. Accuracy of ML model reduced by 4 % after adding noise. This reduction in accuracy is mainly due to misclassification around lower frequency range (100-1000 Hz). Performance of trained model is tested under worst condition since noise is only added during the test stage. Performance of trained model can be improved if presence of noise is also considered at the training stage.

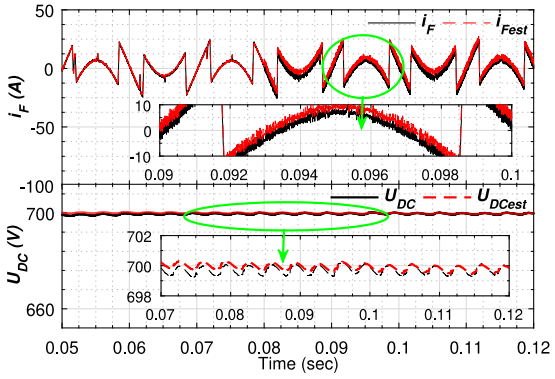

FIGURE 18. Actual and estimated quantities: Filter current (i_F) and DC voltage (U_{DC}) from top to bottom respectively.

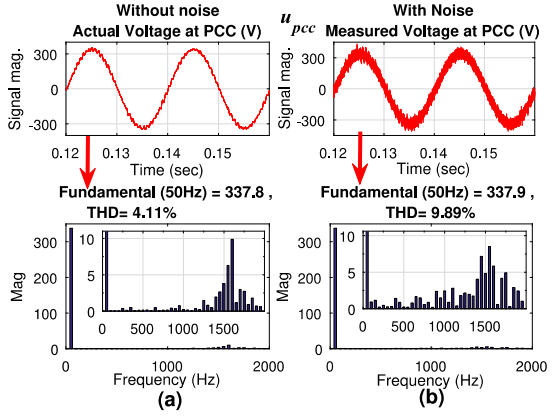

FIGURE 19. FFT Analysis of PCC voltages (phase a): (a) Without noise, (b) with noise.

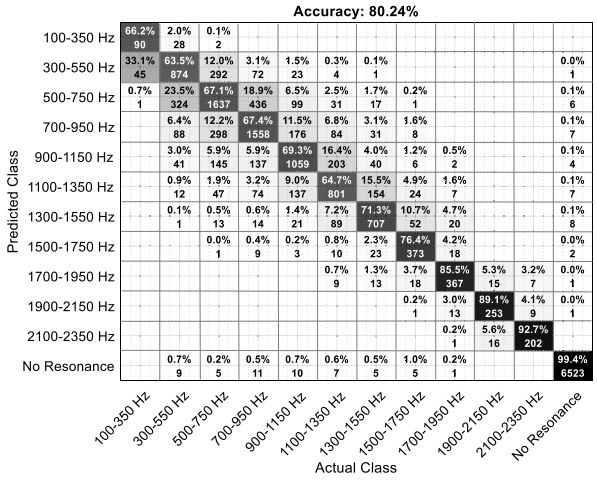

FIGURE 20. Confusion matrix showing performance of SVM trained model for test data containing noise.

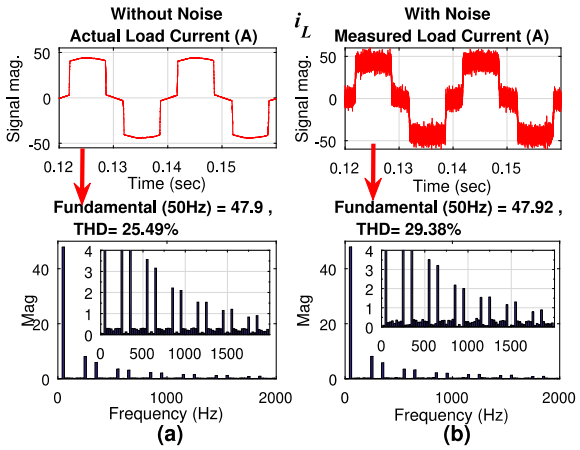

FIGURE 21. FFT Analysis of load current (phase a): (a) Without noise, (b) with noise.

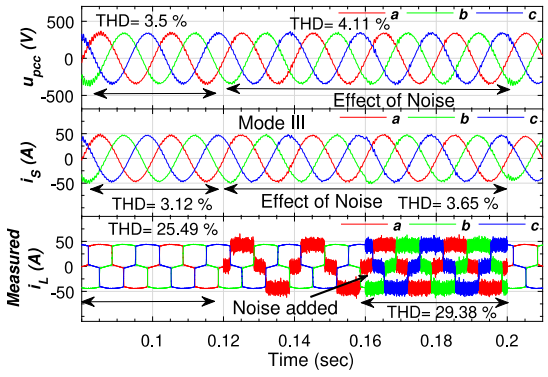

FIGURE 22. Performance of SAPF in presence of noise in load current measurement.

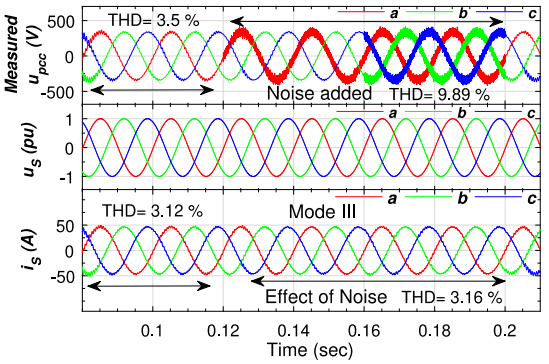

FIGURE 23. Performance of SAPF in presence of noise in PCC voltage measurement.

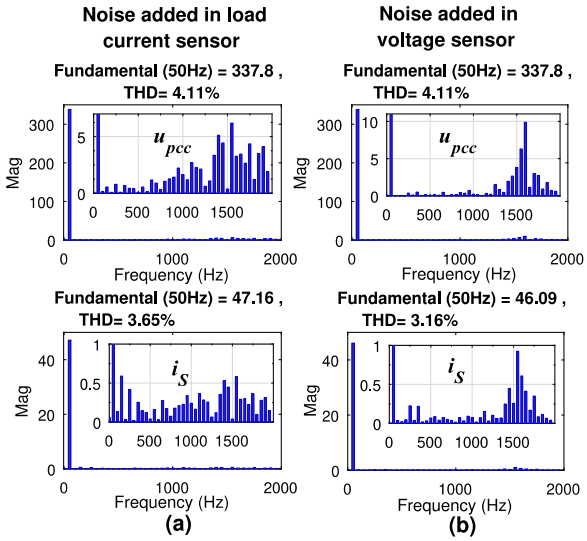

FIGURE 24. FFT Analysis of voltage at PCC and load current (phase a) in presence of:- (a) noise in load current measurement, (b) noise in PCC voltage measurement.

2) EFFECT OF NOISE ON RESONANCE DAMPING AND HARMONIC COMPENSATION

Combined control strategy requires information from PCC voltage and load current sensor. Here, SAPF is operating in Mode III under case 2 condition i.e., SAPF is performing both harmonic compensation and resonance damping and resonance at around 1550 Hz is considered for evaluation. It can be observed from Fig.21 that THD of load current increased from 25.49 % to 29.38 % on adding noise. From t = 0.12 to 0.2 sec, white noise is added in phase *a* sensor of load current and from t = 0.16 to 0.2 sec, noise is added in all three phase sensors of load current as shown in Fig.22. The presence of noise resulted in an increase in THD of i_S from 3.12 % to 3.65 % during t = 0.12 to 0.2 sec. Similarly, for PCC voltage sensors, white noise is added in phase '*a*' sensor of PCC voltage from t = 0.12 to 0.2 sec and in all three phases from t = 0.16 to 0.2 sec as shown in Fig. 23. This voltage is shown with "$Measured u_{pcc}$" i.e., measured PCC voltage which is involved in the reference current generation technique. From the source current waveform shown in Fig. 23, it can be observed that performance of SAPF is not significantly affected in presence of noise in PCC voltage sensor. THD of source current only increased from 3.12 % to 3.16 %. This is because unit voltage generation remained unaffected in presence of disturbance in voltage

sensors as shown by u_S waveform in Fig. 23. Corresponding FFT analysis of PCC voltage and source current in presence of load current and voltage sensor noise is shown in Fig. 24 (a) and (b) respectively.

VI. CONCLUSION

This paper proposes a new technique to detect resonance in power distribution system. This technique is based on the machine learning based classification approach, which utilizes both KNN as well as SVM algorithm. Machine learning approach solves the problem of external signal injection, complex algorithms and additional circuitry which is usually required to detect harmonic resonance. This paper also provides an insight into various possible cases of resonance caused due to different parameters in the distribution network consisting of both SAPF and a PFC capacitor bank. A realistic database resembling the behaviour of the actual resonance cases in power distribution network is created such that it consists of a variety of resonance scenarios with different characteristics, e.g., resonance frequency, amplification factor and bandwidth. Resonance frequency within 2.5 kHz is detected while considering the bandwidth of 250 Hz. Accuracy of 84% from SVM and 78 % from KNN is obtained for classifying the test data.

This paper deals with the classification and detection of resonance in terms of different frequency ranges. Further research will focus on resonance identification in terms of amplification factor through machine learning. In addition to this, further testing with real field measurement data is required to assess the accuracy of the machine learning-based detection approach in detecting/classifying practical resonance scenarios.

In addition to resonance detection, resonance damping and harmonic compensation are achieved by utilising only two sensors thus reducing the overall requirement of dedicated sensors.

ACKNOWLEDMENT

Princess Nourah bint Abdulrahman University Researchers Supporting Project number (PNURSP2022R79), Princess Nourah bint Abdulrahman University, Riyadh, Saudi Arabia.

REFERENCES

[1] C. Jie, L. Long-Fu, L. Yong, and C. Gui-Ping, "Study on harmonic resonance mechanism and its suppression method in isolated network system," in *Proc. 13th IEEE Conf. Ind. Electron. Appl. (ICIEA)*, May 2018, pp. 2625–2630.

[2] S. Liu, F. Lin, X. Fang, Z. Yang, and Z. Zhang, "Train impedance reshaping method for suppressing harmonic resonance caused by various harmonic sources in trains-network systems with auxiliary converter of electrical locomotive," *IEEE Access*, vol. 7, pp. 179552–179563, 2019.

[3] A. S. Koch, J. M. A. Myrzik, T. Wiesner, and L. Jendernalik, "Harmonics and resonances in the low voltage grid caused by compact fluorescent lamps," in *Proc. 14th Int. Conf. Harmon. Qual. Power (ICHQP)*, Sep. 2010, pp. 1–6.

[4] B. Singh, K. Al-Haddad, and A. Chandra, "A review of active filters for power quality improvement," *IEEE Trans. Ind. Electron.*, vol. 46, no. 5, pp. 960–971, Oct. 1999.

[5] J. C. Das, "Harmonic resonance," in *Power System Harmonics and Passive Filter Designs*. Hoboken, NJ, USA: Wiley, 2015, pp. 379–425.

[6] B. Xie, L. Zhou, and M. Mao, "Analysis of resonance and harmonic amplification for grid-connected inverters," *IET Gener., Transmiss. Distrib.*, vol. 13, no. 10, pp. 1821–1828, May 2019.

[7] R. Kumar and H. O. Bansal, "Shunt active power filter: Current status of control techniques and its integration to renewable energy sources," *Sustain. Cities Soc.*, vol. 42, pp. 574–592, Oct. 2018.

[8] H. Saxena, A. Singh, and J. N. Rai, "Design and performance analysis of improved Adaline technique for synchronization and load compensation of grid-tied photovoltaic system," *Int. Trans. Electr. Energy Syst.*, vol. 30, no. 6, pp. 1–18, Jun. 2020.

[9] E. Sundaram, M. Gunasekaran, R. Krishnan, S. Padmanaban, S. Chenniappan, and A. H. Ertas, "Genetic algorithm based reference current control extraction based shunt active power filter," *Int. Trans. Electr. Energy Syst.*, vol. 31, no. 1, pp. 1–22, Jan. 2021.

[10] Q. Wu, K. Dai, X. Chen, Y. Zhang, C. Xu, and Z. Dai, "Reactive current reshaping with series resonance damping for three-phase buck-type dynamic capacitor," *IEEE Access*, vol. 7, pp. 142663–142674, 2019.

[11] D. Detjen, J. Jacobs, R. W. De Doncker, and H.-G. Mall, "A new hybrid filter to dampen resonances and compensate harmonic currents in industrial power systems with power factor correction equipment," *IEEE Trans. Power Electron.*, vol. 16, no. 6, pp. 821–827, Nov. 2001.

[12] H. Fujita, T. Yamasaki, and H. Akagi, "A hybrid active filter for damping of harmonic resonance in industrial power systems," *IEEE Trans. Power Electron.*, vol. 15, no. 2, pp. 215–222, Mar. 2000.

[13] B. G. Lemma and M. Liao, "Active impedance-based single-phase hybrid active power filter," *IEEJ Trans. Electr. Electron. Eng.*, vol. 14, no. 9, pp. 1381–1388, 2019.

[14] T. Lee, Y. Wang, J. Li, and J. M. Guerrero, "Hybrid active filter with variable conductance for harmonic resonance suppression in industrial power systems," *IEEE Trans. Ind. Electron.*, vol. 62, no. 2, pp. 746–756, Feb. 2015.

[15] Z. Fang, W. Longhui, C. Zhe, W. Xianwei, and W. Zhaoan, "Study on a control method of PAPF for resonance damping and harmonics compensation in power system," in *Proc. IEEE 6th Int. Power Electron. Motion Control Conf.*, May 2009, pp. 1161–1167.

[16] A. Cleary-Balderas and A. Medina-Rios, "Harmonic resonance damping on capacitor bank filters for industrial power system applications," in *Proc. IEEE Int. Autumn Meeting Power, Electron. Comput. (ROPEC)*, Nov. 2017, pp. 1–5.

[17] C. Liu, Y. He, K. Dai, and Y. Kang, "Industrial power distribution system harmonic resonance problem and solution with shunt active power filter," in *Proc. 43rd Annu. Conf. IEEE Ind. Electron. Soc. (IECON)*, Oct. 2017, pp. 1243–1248.

[18] T.-L. Lee and S.-H. Hu, "An active filter with resonant current control to suppress harmonic resonance in a distribution power system," *IEEE J. Emerg. Sel. Topics Power Electron.*, vol. 4, no. 1, pp. 198–209, Mar. 2016.

[19] W. Yeetum and V. Kinnares, "Parallel active power filter based on source current detection for antiparallel resonance with robustness to parameter variations in power systems," *IEEE Trans. Ind. Electron.*, vol. 66, no. 2, pp. 876–886, Feb. 2019.

[20] A. Bottenberg, C. Debruyne, B. Peterson, J. Rens, J. Knockaert, and J. Desmet, "Network resonance detection using harmonic active power," in *Proc. 18th Int. Conf. Harmon. Qual. Power (ICHQP)*, May 2018, pp. 1–5.

[21] C. Xu, K. Dai, X. Chen, L. Peng, Y. Zhang, and Z. Dai, "Parallel resonance detection and selective compensation control for SAPF with square-wave current active injection," *IEEE Trans. Ind. Electron.*, vol. 64, no. 10, pp. 8066–8078, Oct. 2017.

[22] A. Riccobono, M. Mirz, and A. Monti, "Noninvasive online parametric identification of three-phase AC power impedances to assess the stability of grid-tied power electronic inverters in LV Networks," *IEEE J. Emerg. Sel. Topics Power Electron.*, vol. 6, no. 2, pp. 629–647, Jun. 2018.

[23] P. G. V. Axelberg, I. Y. H. Gu, and M. H. J. Bollen, "Support vector machine for classification of voltage disturbances," *IEEE Trans. Power Del.*, vol. 22, no. 3, pp. 1297–1303, Jul. 2007.

[24] D. C. P. Barbosa, V. L. Tarrago, L. H. A. de Medeiros, M. T. de Melo, L. R. G. da Silva Lourenco Novo, M. D. S. Coutinho, M. M. Alves, H. B. D. T. L. Neto, P. H. R. P. Gama, and R. G. M. dos Santos, "Machine learning approach to detect faults in anchor rods of power transmission lines," *IEEE Antennas Wireless Propag. Lett.*, vol. 18, no. 11, pp. 2335–2339, Nov. 2019.

[25] H. Liu, F. Hussain, S. Yue, O. Yildirim, and S. J. Yawar, "Classification of multiple power quality events via compressed deep learning," *Int. Trans. Electr. Energy Syst.*, vol. 29, no. 6, pp. 1–14, Jun. 2019.

[26] G. Goswami and P. K. Goswami, "Power quality improvement at nonlinear loads using transformer-less shunt active power filter with adaptive neural fuzzy interface system supervised PID controllers," *Int. Trans. Electr. Energy Syst.*, vol. 30, no. 7, pp. 1–14, 2020.
[27] W. Lee, "Supervised learning-classification using K-nearest neighbors (KNN)," in *Python Machine Learning*. Hoboken, NJ, USA: Wiley, 2019, pp. 205–220.
[28] W. Lee, "Supervised learning-classification using support vector machines," in *Python Machine Learning*. Hoboken, NJ, USA: Wiley, 2019, pp. 177–203.
[29] Q. Liu, J. Li, and W. Mingli, "Field tests for evaluating the inherent high-order harmonic resonance of traction power supply systems up to 5000 Hz," *IEEE Access*, vol. 8, pp. 52395–52403, 2020.
[30] B. Singh and J. Solanki, "An implementation of an adaptive control algorithm for a three-phase shunt active filter," *IEEE Trans. Ind. Electron.*, vol. 56, no. 8, pp. 2811–2820, Aug. 2009.
[31] D. A. Adeniyi, Z. Wei, and Y. Yongquan, "Automated web usage data mining and recommendation system using K-nearest neighbor (KNN) classification method," *Appl. Comput. Inform.*, vol. 12, no. 1, pp. 90–108, Jan. 2016.
[32] W. C. Hsu and T. Y. Yu, "E-mail spam filtering based on support vector machines with Taguchi method for parameter selection," *J. Converg. Inf. Technol.*, vol. 5, no. 8, pp. 78–88, Oct. 2010.
[33] S. Sharma and V. Verma, "Modified control strategy for shunt active power filter with MRAS-based DC voltage estimation and load current sensor reduction," *IEEE Trans. Ind. Appl.*, vol. 57, no. 2, pp. 1652–1663, Apr. 2021.
[34] S. Sharma, V. Verma, and R. K. Behera, "Real-time implementation of shunt active power filter with reduced sensors," *IEEE Trans. Ind. Appl.*, vol. 56, no. 2, pp. 1850–1861, Mar. 2020.
[35] *IEEE Recommended Practice and Requirements for Harmonic Control in Electric Power Systems*, IEEE Standard 519-2014 (Revision of IEEE Std 519-1992), 2014, pp. 1–29.

SHIVANGNI SHARMA received the B.Tech. degree in electrical engineering from Dr. A. P. J. Abdul Kalam Technical University, Lucknow, India, in 2014. She is currently pursuing the dual M.Tech. and Ph.D. degree with the Department of Electrical Engineering, NIT Patna, Patna, India.

Her research interests include power electronics, sensorless control, and power quality issues.

VIMLESH VERMA (Senior Member, IEEE) was born in Mumbai, India. He received the B.Tech. degree in electrical and electronics engineering from Andhra University, Visakhapatnam, India, in 2002, the M.Tech. degree in power apparatus and systems from Nirma University, Ahmedabad, India, in 2005, and the Ph.D. degree in electrical engineering from the Indian Institute of Technology Kharagpur, Kharagpur, India, in 2015.

He is currently an Assistant Professor with the Department of Electrical Engineering, National Institute of Technology Patna, Patna, India. His research interests include the sensorless control of ac drives, fault diagnosis, motor drives, power converters, electric vehicles, and renewable energy.

MOHD TARIQ (Senior Member, IEEE) received the bachelor's degree in electrical engineering from Aligarh Muslim University, Aligarh, the master's degree in machine drives and power electronics from the Indian Institute of Technology (IIT) Kharagpur, and the Ph.D. degree in electrical engineering with a focus on power electronics and control from Nanyang Technological University (NTU), Singapore.

He is currently working as an Assistant Professor with Aligarh Muslim University, where he is directing various international and national sponsored research projects and leading a team of multiple researchers in the domain of power converters, energy storage devices, and their optimal control for electrified transportation and renewable energy application. Previously, he worked as a Researcher at Rolls-Royce-NTU Corporate Laboratory, Singapore, where he worked on the design and development of power converters for more electric aircraft. Before joining his Ph.D., he worked as a Scientist with the National Institute of Ocean Technology, Chennai, under the Ministry of Earth Sciences, Government of India, where he worked on the design and development of BLDC motors for the underwater remotely operated vehicle application. He worked as an Assistant Professor at the Maulana Azad National Institute of Technology (MANIT), Bhopal, India. He has secured several fundings worth approximately 18 million INR. He has authored more than 180 research papers in international journals/conferences, including many articles in IEEE TRANSACTIONS/journals. He is also an inventor of approximately 25 patents granted/published by the patent offices of USA, Australia, U.K., EP, India, and China.

Dr. Tariq was a recipient of the 2019 Premium Award for Best Paper in *IET Electrical Systems in Transportation* journal for his work on more electric aircraft and also the Best Paper Award from the IEEE Industry Applications Society's (IAS) and the Industrial Electronic Society (IES), Malaysia Section - Annual Symposium (ISCAIE-2016) held in Penang, Malaysia, and many other best paper awards in different international conferences. He is a Young Scientist Scheme Awardee (2019) supported by the Department of Science and Technology, Government of India, a Young Engineer Awardee (2020) by the Institution of Engineers (India), and a Young Researcher Awardee (2021) by the Innovation Council, AMU. He is also the Founder Chair of the IEEE AMU Student Branch and the Founder Chair of the IEEE SIGHT AMU.

SHABANA UROOJ (Senior Member, IEEE) received the B.E. degree in electrical engineering and the M.Tech. degree in instrumentation and control from Aligarh Muslim University, Aligarh, India, in 1998 and 2003, respectively, and the Ph.D. degree from the Department of Electrical Engineering, Jamia Millia Islamia (A Central University), Delhi, India, in 2011.

She has nearly three years of industry experience and over 19 years of teaching experience. She is currently working as an Associate Professor with the Department of Electrical Engineering, College of Engineering, Princess Nourah bint Abdulrahman University, Riyadh, Saudi Arabia. She has guided several Ph.D. and master's thesis and dissertations. She has authored or coauthored more than 150 research papers which are published in high quality international journals and conference proceedings. She was a recipient of the Research Excellence Award from PNU, the Springer's Excellence in Teaching and Research Award, the American Ceramic Society's Young Professional Award, the IEEE Region 10 Award for Outstanding Contribution in Educational Activities, and several best paper presentation awards. Recently, she has received the Badge of IEEE STEM Ambassador for her Excellent Volunteering and Efforts in STEM Promotional Activities. She is holding the responsibility of the Vice Chair of the IEEE Saudi Arabia Section.